Cellulose (2023) 30:9647–9667
https://doi.org/10.1007/s10570-023-05453-9

ORIGINAL RESEARCH

# Aerenchyma tissue of *Juncus effusus* L.: a novel resource for sustainable natural cellulose foams

**Qi Chen · Jur van Dijken · Dina Maniar · Katja Loos**

Received: 13 January 2023 / Accepted: 12 August 2023 / Published online: 12 September 2023


**Abstract** The demand for sustainable, low-cost, and high-performance natural cellulose foams with isotropic structures has increased greatly due to growing environmental awareness. However, the synthesis of current cellulose foams/aerogels requires substantial amounts of energy and chemicals, mainly due to the challenges posed by the poor solubility and processability of raw cellulose derived from biomass resources. Consequently, these challenges further highlight the advantages offered by the direct utilization of natural cellulose foams, considering their economic and environmental benefits. Previous studies on natural cellulose foams have predominantly focused on specific plant components such as phloem, xylem, vascular vessels, fruits, and seeds. In this study, we present an overlooked alternative: the aerenchyma tissue of aquatic or wetland plants. Specifically, we investigated on *Juncus effusus* L. (JE), a commonly found problematic wetland weed that is known for its high reproductive ability, causing a reduction in annual forage yield. The aerenchyma tissue of JE was discovered to possess a well-developed 3D interconnected hierarchical structure, exhibiting remarkable properties as a natural lignocellulosic foam. These properties include exceptional compressibility, hydrophobicity (water contact angle: 147°), lightweights (density: 0.017 g/cm$^3$), and high porosity (98%). Through this study, we have introduced a novel natural cellulose foam and explored the utilization of biomass derived from wetland weed wastes.

**Keywords** *Juncus effusus* L. · Wetland weed · Aerenchyma · Cellulosic foam · Hollow fibers

Q. Chen · J. van Dijken · D. Maniar · K. Loos (✉)
Macromolecular Chemistry and New Polymeric Materials, Zernike Institute for Advanced Materials, University of Groningen, Nijenborgh 4, 9747 AG Groningen, The Netherlands
e-mail: k.u.loos@rug.nl

## Introduction

Natural fibers attract a lot of attention in research and industry, due to their biodegradability, biocompatibility, versatility and ubiquity (Seki et al. 2022). Apart from the general cellulosic fibers extracted from various plants utilized as textiles, artwork, thermoplastic reinforcement composites (Sanjay et al. 2019), or other value-added products (Nascimento et al. 2021; Rajeshkumar et al. 2021; Elseify et al. 2022; Sanjay et al. 2022), cellulosic foams with three-dimensional hierarchical structures have been increasingly appreciated by researchers recently. For example, cellulosic sponges/aerogels were widely applied in oil/water separation (Thilagavathi et al. 2018; Datiles et al. 2021; Chen et al. 2023a), nanogenerators (Zhang et al. 2021; Ram et al. 2021), dye adsorption (Fauziyah et al. 2019; Xia et al. 2020a), thermal insulation (Sen et al. 2022), packaging (Miranda-Valdez et al. 2023), biomedical applications (Zampieri et al. 2006;

Seddiqi et al. 2021), and as carbon source/template for electrochemical devices (Sun et al. 2019). Based on recent reviews (Budtova 2019; Rahmanian et al. 2021; Zaman et al. 2020), cellulosic foams can be categorized into two groups: synthetic cellulose aerogels and natural cellulose foams. The solubility and processability of raw natural cellulose derived from biomass resources pose inherent limitations in the production of synthetic cellulose aerogels. Additional treatments are often required prior to the freeze-/supercritical-drying of the cellulose composites (Vinod et al. 2020). These treatments include extraction processes (e.g. high-frequency ultrasonic crushing, mechanical stirring, high-pressure homogenization, TEMPO oxidation, acid hydrolysis, or bacterial secretion) (Manian et al. 2021; Mokhena and John 2020), or regenerated processes in various solvents (e.g. ionic liquids, *N*-methylmorpholine-*N*-oxide (NMMO), LiCl/DMAc systems, or alkali/urea aqueous solutions). Consequently, substantial amounts of energy and chemicals are required to process raw natural cellulose into synthetic cellulose aerogel. In terms of cost and environmental impact, it is therefore more attractive to consider directly utilizing natural cellulose foams. Until now, sources of reported cellulosic foams have been limited to the plant components such as phloem (hemp), xylem (balsa wood), vascular vessels (sugarcane bagasse), fruits (luffa cylindrica) and seeds (kapok or poplar catkins) (Pennells et al. 2020). Additionally, foam structures derived from these sources are primarily tubular in nature (e.g., hemp, cotton, kapok, poplar catkins, and coir) or honeycomb-like, as observed in balsa wood or cork. However, there are limited reports on naturally occurring cellulose foams that possess regularly interconnected networks (Bismarck et al. 2002; Chen et al. 2013; Cruz et al. 2013; Shen et al. 2013; Zhang et al. 2020a). Therefore, there is an urgent and compelling need to explore additional sources of natural cellulose foams that are cost-effective and exhibit high-performance. It is also crucial to discover novel foam structures (Li et al. 2021). Hence, the study of plant tissue with unique structures, such as aerenchyma, holds significant potential and garners considerable interest.

Aerenchyma tissue is considered to be the most striking morphological feature within plants. It is commonly found in aquatic and wetland species, assisting with their floating and internal air circulation (Blossfeld et al. 2011). This unique foamy tissue, which serves to retain air, is predominantly composed of aerenchymatic channels that possess large intercellular spaces, contributing to the high porosity of the aerenchyma. The arrangement of aerenchymatic channels exhibits distinct patterns in various plant species, including the radial arrangement in *Ceratophyllum demersum*, the perpendicular arrangement in *Myriophyllum aquaticum*, the honeycomb arrangement in water hyacinth, and the stellate network in *Juncus effusus* L. (Justin and Armstrong 1987). These aquatic plants show a high reproductive ability and possess sophisticated aerenchyma tissue, which can potentially be applied for water purification (Wolverton and Mcdonald 1979; Keskinkan et al. 2004; Xia et al. 2020a; Guo et al. 2020). On the other hand, they are also assessed as hard-to-handle weeds—controlling their quantities costs millions of dollars annually (Wolverton and Mcdonald 1979; Kaczmarek-derda et al. 2014). Thus, utilizing aerenchyma tissue as a natural cellulose foam resource offers a practical and valuable solution that addresses three interconnected problems. Firstly, it enables the utilization of abundant prolific wetland/aquatic pests. Secondly, it contributes to the promotion of biodiversity by exploring novel natural foam sources. Lastly, it leads to the discovery of natural foam structures. However, turning these weeds into an added-value product requires an in-depth study of their characteristics. Here, the aerenchyma tissue of *Juncus effusus* L. with the extraordinary stellate network was selected and characterized for its further potential foam applications such as oil adsorption, water purification, nanogenerator (Chen et al. 2023b) or foam structural templates.

*Juncus effusus* L. is a wetland perennial monocot, distributed widely throughout warm temperature zones in Eurasia and the American continents as one of the dominant species in multiple altitude ranges (Tweed and Woodhead 1946). Due to its high seed production and faster regrowth rate outcompeting neighboring species, *Juncus effusus* L. has the annual production of ~ 10 kg ash-free dry mass (AFDM) per $m^2$ (Ervin and Wetzel 2002). Consequently, it is considered as a problematic weed in pastures and meadows as it impairs the forage yield and quality (Lazenby 1955; Kaczmarek-derda et al. 2014). According to the literature, the epidermis of their stem was usually utilized in weave while their pith was historically applied as wicks in train-oil lamps

across north-western Europe and China (Kaczmarek-derda et al. 2018), or as traditional Chinese medicine (Noguchi et al. 2017). Recently, it was utilized in solar-driven steam generators (Zhang et al. 2020b) and soluble pollutant removals (Xia et al. 2020a). Nevertheless, comprehensive characterization studies of the pith aerenchyma foam in *Juncus effusus* L. (JEF) and the separation of its structural stellate unit have not yet been reported. This work aims to assess the potential usage of *Juncus effusus* L. pith aerenchyma as 3-dimensional flexible cellulosic foams, and to provide a new structure template for lightweight highly porous materials.

The structural, physico-chemical, mechanical and thermal characteristics of delignified stellate units of JEF and raw JEF were comprehensively analyzed. The properties of JEF were evaluated via single fiber tensile tests, cyclic compression tests, $N_2$ adsorption–desorption experiments, liquid immersion tests, water contact angle measurements (WCA), chemical analysis, Scanning Electron Microscope (SEM) observations, X-ray diffraction (XRD), Fourier transform infrared spectroscopy (FTIR) and Thermogravimetric analysis (TGA). The properties were compared with other natural lignocellulosic foams.

## Materials and methods

### Fibers obtainment

*Juncus effusus* L. stems were collected from the Sprikkenburg riverside (53° 14′ N, 6° 31′ E) as shown in Fig. 1a within the university complex in Groningen. The stems were cut to 50 cm in length and their outer green epidermis was subsequently peeled off manually with a tweezer (Fig. 1c). The obtained JE aerenchyma foam (JEF in Fig. 1c) was kept in an air oven at 105 ℃ overnight to remove the moisture for further characterizations.

## Characterization methods

### Morphological characterization

The collected JE stems were divided into young and old groups (Fig. 1b) according to the color of the stem and the size of central lacunas. The morphological characteristics of these two kinds of stems were investigated by scanning electron microscopy (SEM) via a FEI Nova NanoSEM 650 with an accelerating voltage of 15 kV. Samples were coated with 10 nm Au in a Cressington

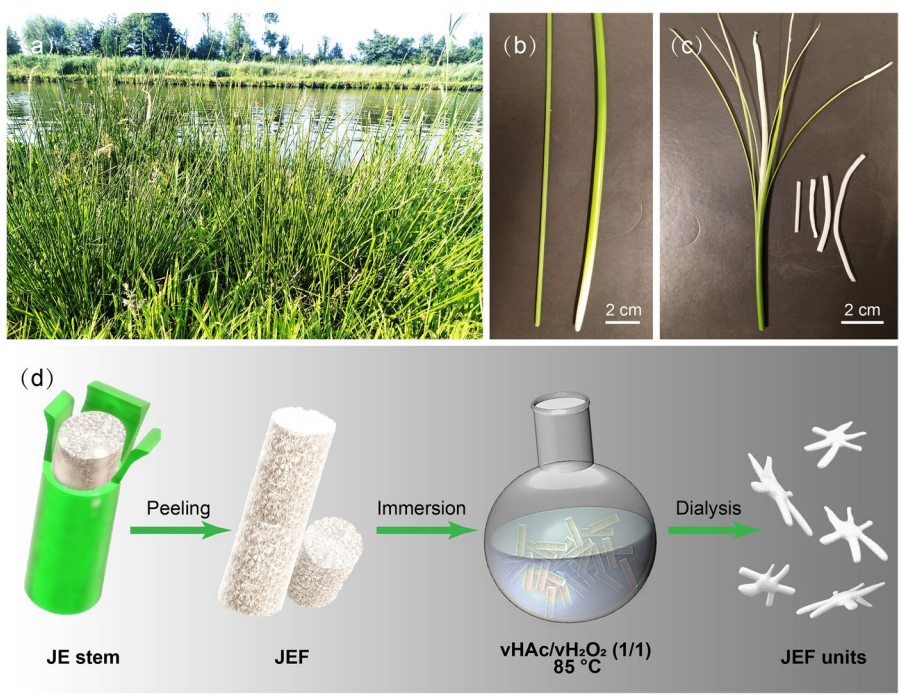


**Fig. 1** **a** *Juncus effuses* L., **b** old (left) and young (right) JE stems, **c** JEF extracted from young JE stems, **d** schematic illustration of JEF unit's separation process

Sputter Coater 208HR before imaging. The JEF diameter ($D$) and JEF units' parameters in Table 2 were calculated from SEM images using the software ImageJ 1.53a. A total of 5 samples were measured in 20 different spots. The JEF stellate units' cellulose crystals were studied by polarized optical microscopy (POM). A Zeiss Axiophot polarizing microscope equipped with a Sony DICC-500 camera for image acquisition was used and the images of bright field and POM were all recorded by Zeiss KS3000 software.

## Density and porosity measurements

The solid density ($\rho_s$) was obtained by liquid immersion test using a pycnometer (Blaubrand, Gay-Lussac) with toluene at 20 °C (Siva et al. 2020). The $\rho_s$ (g/cm$^3$) of JEF was calculated via Eq. (1) (Lee et al. 1983):

$$\rho_s = \frac{(m_2 - m_1)}{(m_3 - m_1)(m_4 - m_2)}\rho_t \quad (1)$$

where, $\rho_t$ is the density of toluene at 20 °C (0.867 g/cm$^3$), $m_1$ represents the mass of the empty pycnometer (g), $m_2$ is the mass of pycnometer with JEF (g), $m_3$ is the mass of pycnometer filled with toluene (g) and $m_4$ is the mass of a pycnometer with JEF and toluene (g).

The bulk density ($\rho_b$) of JEF (g/cm$^3$) was determined via Eq. (2):

$$\rho_b = \frac{m}{V} \quad (2)$$

where $m$ is the mass of JEF (g) and $V$ is the calculated volume of JEF while regarding them as the cylindrical shape.

With the obtained values of $\rho_s$ and $\rho_b$, the porosity $P$ of JEF could be estimated via Eq. (3):

$$P = \left(1 - \frac{\rho_b}{\rho_s}\right) \times 100 \quad (3)$$

The obtained density and porosity results are listed in Table 1.

## Chemical composition analysis

The carbohydrate composition analysis was conducted according to the method provided by the National Renewable Energy Laboratory (NREL/TP-510-42618) (Sluiter et al. 2012). The wax content was quantified referring to the standard protocol (Conrad 1944). The obtained data were compared with other reported natural foams and fibers in Table 1 (Anjos et al. 2008; Bismarck et al. 2002; Borrega et al. 2015; Chaiarrekij et al. 2011; Chen et al. 2013; Cruz et al. 2013; Luz et al. 2017; Dhakal et al. 2007; Driemeier et al. 2011; Gowthaman et al. 2018; Guimarães et al. 2009; Guna et al. 2017; Prakash et al. 2018; Hsieh et al. 1996; Leite and Pereira 2017; Likon et al. 2013; Lim and Huang 2007; Mahmood et al. 2005; Meng et al. 2021; Narayanasamy et al. 2020; Pereira 2015; Saeed and Iqbal 2013; Shen et al. 2013; Singh et al. 2013; Xie et al. 2020; Zhang et al. 2020a, 2017; Zheng et al. 2016).

## Delignification treatment

The JEF units were separated via a previously reported delignification method (Sun et al. 2020). As shown in Fig. 1d, g JEF was submerged into a mixture of 50 mL of acetic acid (≥99.7%, Sigma-Aldrich) and 50 mL of hydrogen peroxide (30%, Sigma-Aldrich) at 85 °C overnight. Subsequently, the separated JEF units were dialyzed in deionized water with a dialysis membrane (MWCO 1kD, Spectrum Laboratories, Inc.) for 1 week to remove the chemicals. Finally, the JEF units were naturally dried at ambient temperature.

## Fourier transform infrared spectroscopic analysis

Attenuated Total Reflection-Fourier Transform Infrared (ATR-FTIR) spectra were recorded on a Bruker VERTEX 70 spectrometer equipped with a Platinum-ATR diamond single reflection unit in the range of 4000–500 cm$^{-1}$. Each spectrum was the average of 16 scans collected with a resolution of 4 cm$^{-1}$. Atmospheric compensation and baseline correction of all collected spectra were applied via OPUS spectroscopy software (Bruker Optics v7.0).

## Thermogravimetric analysis

Thermogravimetric analysis (TGA) and DTG were performed using a TA-instruments Discovery TGA

**Table 1** Comparison of the physico-chemical properties of JEF with other reported natural foams and fibers

| Plant | Fiber sources | Chemical compositions | | | | | Structural properties | |
|---|---|---|---|---|---|---|---|---|
| | | Cellulose (%) | Hemi cellulose (%) | Lignin (%) | Wax (%) | Ash (%) | Foam type[a] | Structural component |
| *Juncus effusus* L | Pith aerenchyma | 39.67 | 35.97 | 20.18 | 2.52 | 1.66 | *O* | Interconnected hollow stellate cells |
| Water hyacinth | Petiole aerenchyma | 25.64 | 31.81 | 3.55 | – | – | *C* | Interconnected hollow polygonal cells |
| Hemp | Stem phloem | 67 ~ 78.3 | 5.5 ~ 16.1 | 2.9 ~ 3.7 | 0.8 | 2.1 | Fiber | Cylinder with parallel hollow tubes (CPHTs) |
| Sugarcane bagasse | Stem vascular vessel | 54.9 | 16.52 | 23.3 | – | 2.75 | Fiber | CPHTs |
| *Q. suber* L. cork | Stem bark | 17 | 7 | 16 | 44 | 0.7 | *C* | Honeycomb-like stacked regular / irregular polygonal cells |
| Balsa wood | Stem xylem | 42 ~ 45 | 17 ~ 18 | 22 ~ 24 | – | – | *O* | |
| *A. sisalana* | Leaves vascular vessel | 57 ~ 71 | 16 | 9.5 ~ 13.1 | – | 1 | Fiber | CPHTs |
| Cotton | Seed | 94 | 0 | 0 | 0.8 ~ 1.3 | 1.27 | *O* | Wool-like twisted ribbons |
| Kapok | Seed | 64 | 10 | 13 | 0.8 ~ 1.2 | 1.6 | *O* | Microtubes |
| *C. gigantea* | Seed | 64 | 9.6 | 13 | 1.9 | 3.1 | *O* | Microtubes |
| Poplar catkins | Seed | 41 ~ 44 | 19 ~ 21 | 29 | 4 ~ 9 | – | *O* | Microtubes |
| *Luffa cylindrica* | Fruit | 55 ~ 90 | 8 ~ 22 | 10 ~ 23 | – | 0.4 | *O* | Interconnected random lattices |
| Coir | Fruit | 32 ~ 43 | 0.3 | 40 ~ 45 | – | 1.44 | fiber | CPHTs |

**Table 1** (continued)

| Plant | Fiber sources | Physical properties | | | | | References |
|---|---|---|---|---|---|---|---|
| | | $\rho_s$ (g/cm$^3$) | $\rho_b$ (g/cm$^3$) | Porosity (%) | BET (m$^2$/g) | WCA (°) | |
| *Juncus effusus* L. | Pith aerenchyma | 0.89 | 0.017 | 98.08 | 1.31 | 147 | Present work |
| Water hyacinth | Petiole aerenchyma | 0.99 | 0.217 ~ 0.303 | 69.60 | – | < 90 | Guna et al. (2017), Prakash et al. (2018), Mahmood et al. (2005) |
| Hemp | Stem phloem | - | 1.14 ~ 1.47 | 2.46 | 0.75 | 140 | Bismarck et al. (2002), Dhakal et al. (2007) |
| Sugarcane bagasse | Stem vascular vessel | – | 0.20 ~ 0.25 | – | 0.63 | 90 | Guimarães et al. (2009), Driemeier et al. (2011), Cruz et al. (2013) |
| *Q. suber* L. cork | Stem bark | – | 0.12 ~ 0.20 | 0.55 ~ 22.5 | – | 99 | Anjos et al. (2008), Leite and Pereira (2017) |
| Balsa wood | Stem xylem | 1.47 | 0.06 ~ 0.38 | 85.60 | 0.37 | 0 | Borrega et al. (2015), Zhang et al. (2020a) |
| *A. sisalana* | Leaves vascular vessel | 1.45 | 0.7 ~ 1.33 | 10.85 | – | 72 | Rajkumar et al. (2015) |
| Cotton | Seed | 1.52 | – | – | 0.67 | 93 | Hsieh et al. (1996), Singh et al. (2013), Chen et al. (2013) |
| Kapok | Seed | 1.28 | 0.384[b] | 91[b] | 3.07 | 117 | Chaiarrekij et al. (2011), Chen et al. (2013), Lim and Huang, (2007), Zhang et al. (2017) |
| *C. gigantea* | Seed | 1.29 | – | 94[b] | 1.46 | 129 | Chen et al. (2013), Zheng et al. (2016), Narayanasamy et al. (2020) |
| Poplar catkins | Seed | 3.27 | 0.36[b] | 89[b] | 2.42 | 150 | Likon et al. (2013) |
| *Luffa cylindrica* | Fruit | 0.92 | 0.025 ~ 0.065 | 79 ~ 93 | 6.00 | 119 | Shen et al. (2013), Xie et al. (2020) |
| Coir | Fruit | – | 1.39 ~ 1.52 | 45 ~ 60 | 4.85 | 77 | Luz et al. (2017) |

[a] *O* stands for open-cell foam, and *C* represents closed-cell foam type; [b] void percentage calculated from a single tubular fiber

5500. Samples of approximately 5 mg were heated in a nitrogen environment from room temperature to 800 ℃ (10 ℃/min). Results were collected and analyzed via the software TA instruments Trios v4.3.1.39215.

### X-ray diffraction analysis

X-ray diffraction (XRD) spectra were acquired at room temperature using a Bruker D8 Advance diffractometer (Cu Kα radiation, λ = 0.1542 nm) with a 10.5° divergent slit and a 10.5° anti-scattering slit. The pattern was recorded for 2θ ranging from 10° to 80° in steps of 0.01° and a counting time of 1 s per step, with an intensity of 40 mA and a voltage of 40 kV. For all XRD measurements, approximately 30 mg of JEF samples or isolated JEF units were compressed into a pellet under a dry state using a stress of 12.75 MPa. The environmental background data was also collected under the same measurement conditions with the blank sample holder, which was then subtracted from the data of all experimental samples (Hermans and Weidinger 1948; French 2020). Subsequently, the obtained experimental XRD spectra were fitted with the cellulose Iβ pattern (French 2014) in the software MAUD (Nascimento et al. 2021; Saville et al. 2021). Experimental data of cotton (Kruidvat cosmetic cotton puff) was collected under the same measurement conditions for comparing the crystallinity of the samples.

The crystallinity index (CrI) was calculated according to the empirical Eq. (4) (Segal et al. 1959).

$$CrI = \frac{I_{200} - I_{am}}{I_{200}} \times 100 \quad (4)$$

where $I_{200}$ represents the maximum intensity at 2θ of 22° referring to the cellulose crystalline content, and $I_{am}$ is the minimum intensity at 2θ of 18.5° referring to the amorphous non-crystalline content of cellulose.

The crystallite size (CS) was calculated by using Scherrer's equation as Eq. (5). (Siva et al. 2020)

$$CS = \frac{K\lambda}{\beta \cos\theta} \quad (5)$$

where K is the Scherrer's constant (0.9), λ is the wavelength of the X-ray source (0.1542 nm), $\beta$ is the peak's full-width half maximum (FWHM), and $\theta$ is the corresponding Bragg angle.

### BET surface area analysis

The specific surface area and pore size were detected with a nitrogen adsorption–desorption experiment at 77 K using a Micromeritics ASAP 2420 V2.05 (V2.05 J) porosimeter. Prior to analysis, ~ 1 g JEF samples was degassed at 105 °C for 12 h under vacuum.

### Water contact angle test

The surface wettability of JEF was evaluated by water contact angle (WCA) measurements, using a Dataphysics OCA 25 system. Milli-Q water droplets of 2 μL were deposited directly on the samples automatically, where a camera recorded the pictures and the contact angles were calculated using the Young–Laplace (YL) equation. The WCA was obtained with three tests per sample.

### Tensile and compressibility test

The tensile tests of JEF were conducted using an Instron 5565 0.1kN Series IX tensile tester with a 100 N load cell. Prior to the test, the ends of samples were wrapped with tape to prevent the damage of jaws' clamping. Tests were conducted at various gauge lengths of 10 mm, 20 mm, 30 mm, 40 mm and 50 mm with 10 samples for each gauge length.

The compressive properties of JEF were evaluated with a cyclic compressive method by an Instron 5565 0.1kN Series IX tensile tester. Prior to the measurements, the samples were cut and fitted into a cylindrical Teflon tube ($\varphi$ 15 mm, $h$ 30 mm). Supported by the tube, JEF were placed between the testing plates and compressed with a speed of 1 mm/min to 30% and 60% of their original thicknesses. All tensile and compressive measurements were conducted at room temperature (20 °C) and at a relative humidity of 60%, and all results were collected via the software Merlin V5.50.00.

## Results and discussion

### Morphologies of JE stems

The morphologies of *Juncus effusus* L. (JE) stems with two representative aging degrees were studied

through its epidermis and aerenchyma by scanning electron microscopy (SEM)—see Fig. 2. Since JE is a wetland monocotyledon, its epidermis of stem works as primary photosynthetic carbon-fixing organs instead of the absent leaves (Stebbins and Khush 1961; Hinchliff and Roalson 2009). As a result, its epidermis contains not only the strong sclerenchymatous fibers (Fig. 2c) for mechanical support (Dou et al. 2019; Lo et al. 2004), but also the vascular bundles (Fig. 2a, b) for water, salts and organics transportation within the plant (Eltahir and AbuEReish 2010). It can clearly be seen from Fig. 2a that the vascular bundles are embedded in parenchyma cells, with sclerenchymatous fibers surrounding the outermost part of the stems. As the maturity of the JE stems increased, the size of scalariform vessels within the vascular bundles was enlarged by approximately 70% (27–46 μm), which led to more voids.

In addition, due to the special aquatic habitat of *Juncus effusus* L., their aerenchyma tissue (auriferous parenchyma) was well developed to ensure a continuous oxygen supply in the oxygen-deficient high humidity soils (Blossfeld et al. 2011). Aerenchyma is regarded as a modified parenchyma, which can always be found in the soft parts of aquatic plants such as lotus or water hyacinth (Guna et al. 2017). As for *Juncus effusus* L., apart from the epidermis, its stem is filled with aerenchymatous cells that have a visual resemblance to cotton wool (Fig. 2c). This spongy culm exhibits extensive inter-connected multicellular structures, which contain numerous small regularly shaped air chambers along both transverse and longitudinal directions for gas diffusion and buoyancy support. Obviously, with the increase of the growth time, the programmed death of aerenchymatous cells results in a large central lacuna in the JE stems (Fig. 2b). This structure of thickened vascular bundle fibers and central voids from old JE stems also showed great consistency with previously reported JE stem fibers (Maache et al. 2017).

According to the observation of JE stems with two representative aging degrees, the spongy JE aerenchyma foams (JEF) from young plump stems were selected for the further studies below.

## Morphologies of JEF

JEF of young JE plump stems were characterized by SEM and optical microscopy. It can be observed that JEF is filled with large symmetrical air spaces (Fig. 3a), which make them appear snow-white color (Fig. 1c). This is comparable to aerenchyma tissue from water hyacinth (Salas-Ruiz et al. 2019). The three-dimensional JEF structure is assembled by large layers of similar cross-linked structures, and each layer is formed by regularly interconnecting the

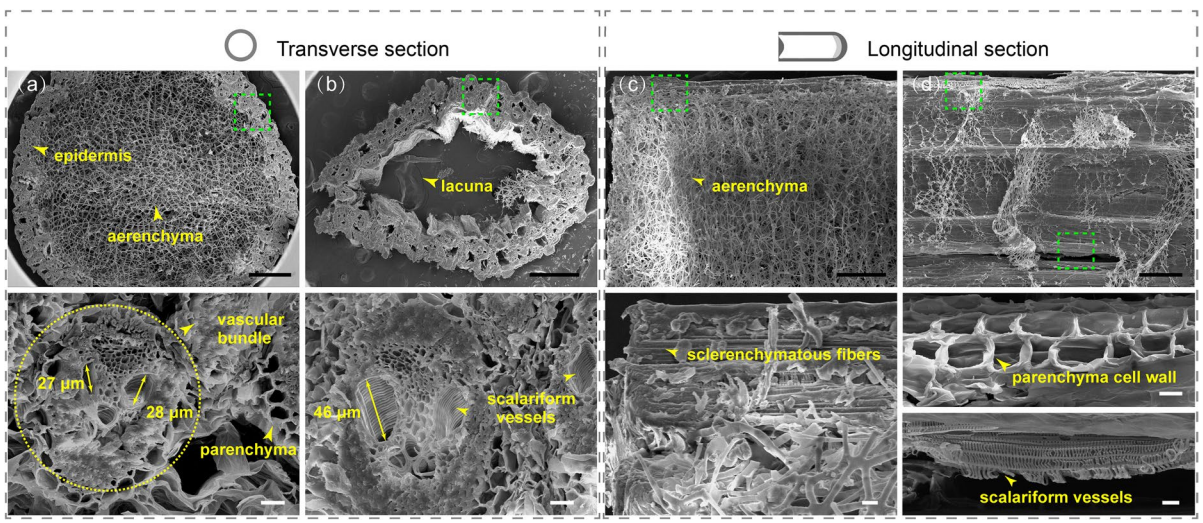


**Fig. 2** SEM images of transverse sections of **a** a young and **b** an old JE stem; SEM images of longitudinal sections of **c** young and **d** old JE stems. The green rectangles in the upper images are shown in higher magnification in their corresponding bottom images. Black and white scale bars here represent 500 μm and 20 μm, respectively

stellate unit (six-rayed stars), which can be seen in Fig. 3f from different directions. The coupling of different layers is achieved via the stellate units' random vertically aligned rays. This hierarchically assembled structure also showed a great similarity with the reported extremely low-density super-compressible graphene foam (Qiu et al. 2017), which might be a hint at its potential as an elastomer in the future. Meanwhile the linkage at the end of each unit can be clearly distinguished from both SEM (Fig. 3d) and bright field optical images (Fig. 3e). Surprisingly, this stellate unit of JEF could be separated while reserving its original structure after the delignification process (Fig. 3c), which showed a great difference with reported shrunken foam structures after alkaline treatment (Xia et al. 2020b). As lignin molecules cross-link different plant poly-saccharides and cellulose, the cell wall's mechanical strength of JEF is enhanced by this process (Chabannes et al. 2001). In contrast to the structure illustrated in Fig. 3b, the stellate unit cell wall showed less stiffness and was inclined to overlap after the delignification process (Fig. 3c), which could be advantageous for further modifications or various lightweight applications.

Interestingly, JEF contained a similar wool-like open-cell foam structure consisting of hollow cylindrical channels as compared with the seed fibers from kapok, *C. gigantea* and poplar catkins (Likon et al. 2013; Zheng et al. 2016). By comparison, JEF stellate units had the narrowest outer diameter *OD* ($7.91 \pm 1.13$ μm) and the shortest channel length *L* ($76.66 \pm 8.77$ μm) among all reported hollow fibers. A more detailed comparison of morphological characteristics of JEF and other typical reported hollow tubular fibers was summarized in Tables 1 and 2. As shown in Table 2, the JEF units contained a similar channel wall thickness *T* ($0.86 \pm 0.18$ μm) as that of *C. gigantea* fibers (0.72 μm), meanwhile it also shared a similar *OD* with poplar catkins fibers ($8.7 \pm 5.7$ μm). In contrast, the *OD* ($16.5 \pm 2.4$ μm) and *T* ($2 \pm 2.4$ μm) of kapok fibers was twice and three times that of JEF units, respectively. On the

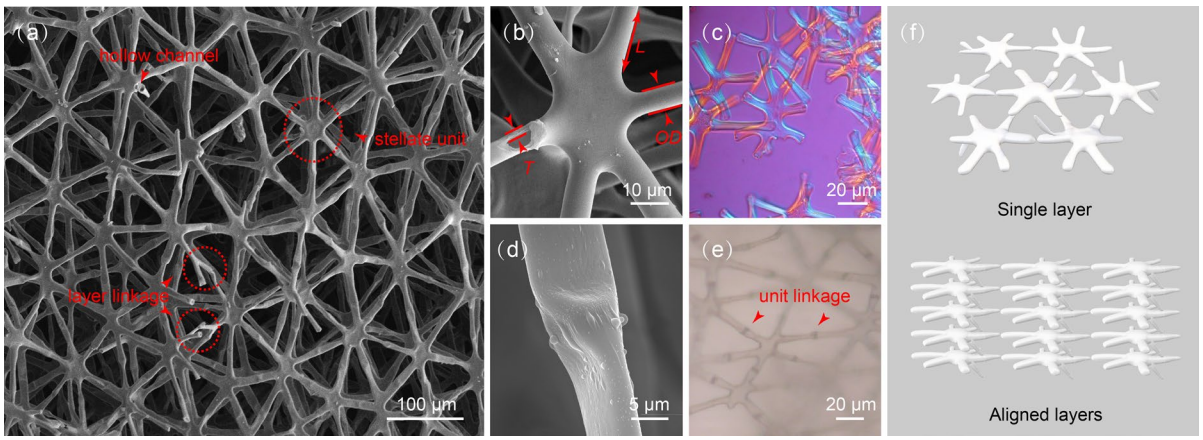


**Fig. 3** SEM images of **a** a JEF network, **b** a JEF stellate unit and **d** the binding parts of the units; Optical microscopy images of **c** delignified JEF stellate units under polarized light and **e** the JEF structure under bright field; **f** schematic structures of JEF interconnected network

**Table 2** Comparison of morphological parameters of JEF units with other typical hollow fibers (Likon et al. 2013; Zheng et al. 2016)

| Unit parameters (μm) | JEF units | Kapok | *C. gigantea* | Poplar catkins |
|---|---|---|---|---|
| Outer diameter (*OD*) | $7.91 \pm 1.13$ | $16.5 \pm 2.4$ | 22.4 | $8.7 \pm 5.7$ |
| Channel wall thickness (*T*) | $0.86 \pm 0.18$ | $2.0 \pm 2.4$ | 0.72 | $0.4 \pm 0.1$ |
| Channel length (*L*) | $76.66 \pm 8.77$ | 15,000 ~ 20,000 | 32,000 | 3000 ~ 5000 |

basis of these hollow channels' morphological differences, the resulting varied cavity ratios further differentiated the bulk densities and porosities of the materials as shown in Table 1. By Comparison, JEF possessed the lowest bulk density (0.017 g/cm$^3$) and the highest porosity (98.08%) among all listed natural lignocellulosic open-cell foams, namely balsa wood (0.06 ~ 0.38 g/cm$^3$ and 85.60%) (Borrega et al. 2015), kapok (0.384 g/cm$^3$ and 91%) (Likon et al. 2013; Thilagavathi et al. 2018), *C. gigantea* (94%) (Thilagavathi et al. 2018), poplar catkins (0.36 g/cm$^3$ and 89%) (Likon et al. 2013; Saeed and Iqbal 2013), and luffa cylindrica (0.025 ~ 0.065 g/cm$^3$ and 79 ~ 93%) (Shen et al. 2013; Saeed and Iqbal 2013). Furthermore, the large amount of air chambers kept within these stacked or interconnected hollow fibers could prevent the entry of liquids with high surface tension (e.g. water), which resulted in their hydrophobic properties. Specifically, poplar catkins fibers showed the highest water contact angle (150°) among all listed natural fibers, and JEF displayed the second highest hydrophobicity (WCA of 147°). The hydrophobic hollow micro-channels of JEF also cause its strong capillary effect for non-polar solvents, which explains why ancient Asians and Europeans used them as wicks for oil lamps (Kaczmarek-derda et al. 2018; Noguchi et al. 2017). Moreover, as density, porosity, hydrophobicity and environmental friendliness play vital roles in oil-absorbing applications, the above-mentioned materials have been reported to exhibit excellent performance as oil absorbents (Datiles et al. 2021; Likon et al. 2013; Liu et al. 2021; Thilagavathi et al. 2018; Yang et al. 2020; Zhang et al. 2017; Zheng et al. 2016). In this case, based on JEF's low density, high porosity and excellent hydrophobicity, it could also be regarded as potential material for adsorption applications or as a lightweight 3D structural template (Manimaran et al. 2018).

## Physico-chemical properties of JEF

### Chemical composition analysis

The chemical composition of natural fibers plays an important role in their mechanical and morphological properties, as well as their thermal stability. Therefore, the chemical composition of JEF was investigated. The obtained results were compared with other reported natural foams and fibers in Table 1. JE contained a similar cellulose content (39.67%) as balsa wood (42 ~ 45%) (Zhang et al. 2020a), poplar catkins (41 ~ 44%) (Likon et al. 2013) and coconut shell coir (32 ~ 43%) (Fiore et al. 2014), while a higher content of cellulose in wet plant water hyacinth aerenchymas can be observed (25.64%) (Guna et al. 2017). The hemicellulose and lignin content of JEF was 35.97% and 20.18%, respectively. This chemical composition ratio demonstrated high similarity to that of Napier grass fibers (cellulose 47.12%, hemicellulose 31.27%, lignin 21.63%) (Kommula et al. 2015). The content of hemicellulose is also similar to that of water hyacinth (31.81%). These considerably high levels of hemicellulose or lignin content can be commonly found in soft grass (Kommula et al. 2015), which necessitates both softness and flexural rigidity to withstand various environmental forces. Hemicellulose, with relatively low mechanical strength, provides the desired softness, while lignin, known for its high mechanical strength, imparts the necessary rigidity (Mohanty et al. 2000; Manimaran et al. 2018). A higher lignin content (20.18%) also helps the plant against biological attack (Manimaran et al. 2018). In addition, the wax content (2.52%) acts as an adhesive between JEF and epidermis in the stem (Jebadurai et al. 2019). At the same time, it serves to protect the stem in aquatic environments due to its hydrophobic nature.

Although the raw JEF foam comprises a mixture of cellulose, hemicellulose, lignin, and wax, each of these components plays a crucial role in the properties of the foam. Specifically, hemicellulose and lignin contribute to its structural integrity, as evidenced by the isolated stellate foam structural units obtained after the delignification process. The presence of wax in JEF also contributes to its high hydrophobicity, thereby expanding its potential applications. Furthermore, the hemicellulose-rich JEF holds great promise as a hemicellulose resource for diverse applications such as hydrogels, thermoplastics, coatings, drug carriers, and additives in food or papermaking (Cunha and Gandini 2010; Fredon et al. 2002; Gabrielii et al. 2000; Jain et al. 2001; Kommula et al. 2015). More importantly, the direct utilization of raw JEF foam allows us to leverage cellulose foam in its natural form, while capitalizing on its inherent excellent foam characteristics (as shown in Table 1). By adopting this approach, we can avoid additional energy/

hazardous chemicals consumption associated with other processes to achieve the true environmental sustainability (from raw materials to manufacturing and final products) (Li et al. 2021). This approach in our study was rooted in the fundamental motivations of utilizing cellulose, with a strong emphasis on energy conservation, sustainability, the abundance of sources, versatility, and cost-effectiveness. These principles were pivotal in driving our efforts to accelerate the transition from the fossil fuel era to a sustainable future.

## ATR-FTIR

FTIR spectra of the raw and delignified JEF units are shown in Fig. 4. The small band centered at 667 $cm^{-1}$ is ascribed to the C–OH out-of-plane bending from cellulose (Pereira et al. 2011; Jaouadi et al. 2009). The band observed at 897 $cm^{-1}$ corresponds to the presence of $\beta$-glycosidic bonds between the monosaccharides (Fiore et al. 2014), which may also indicate the existence of saline content in JEF, according to literature (Khan and Drzal 2004; Sreenivasan et al. 2011). The highest band of 1032 $cm^{-1}$ refers to the alkoxy C–O bond bending vibration and O–H stretching of polysaccharides in cellulose (Prasad et al. 2010; Saravanakumar et al. 2013; Maepaac et al. 2015). The band at 1159 $cm^{-1}$ represents the presence of strong and broad C–OH stretching of cellulose in JEF (Binoj et al. 2016). In addition, the band at 1315 $cm^{-1}$ is attributed to the $CH_2$ asymmetric stretch vibration in crystallized cellulose I (Colom et al. 2003), and the band at 1421 $cm^{-1}$ is assigned to the $CH_2$ bending vibration at $–OCH_3$, representing

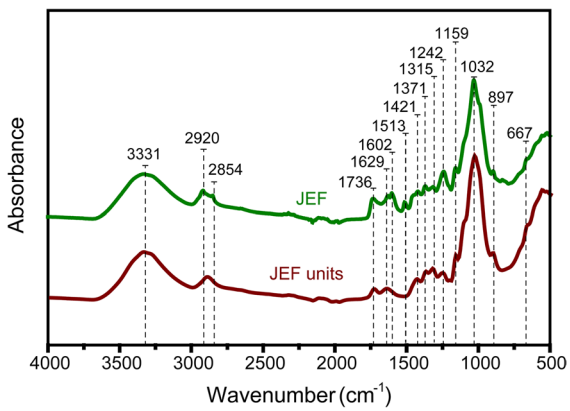


**Fig. 4** FTIR of JEF and JEF units

both crystalline cellulose I and amorphous cellulose (Huang et al 2012). The detection of the band at 1602 $cm^{-1}$ represents the C=C aromatic stretching with strong conjugated C–C bonds in the lignin content (Saravanakumar et al. 2013), while it was also reported to indicate the moisture from natural fibers (Karbowiak et al. 2011). Meanwhile, water trapped in lignin or cellulose can be observed at 1629 $cm^{-1}$, which was usually reported to be present between 1620 $cm^{-1}$ and 1640 $cm^{-1}$ (Nascimento et al. 2021; Boukir et al. 2019). Similarly, the band at 1513 $cm^{-1}$ also refers to the presence of lignin, which can be concluded from the vibrations of C=C groups (Sugiyama et al. 1991). The main bands associated with hemicellulose were expressed at 1242 $cm^{-1}$, 1371 $cm^{-1}$ and 1736 $cm^{-1}$. Specifically, bands at 1242 $cm^{-1}$ corresponds to the syringyl nuclei and C–O stretching in hemicellulose and lignin (Nascimento et al. 2021; Boukir et al. 2019), 1371 $cm^{-1}$ is assigned to the $CH_3$ symmetric bending vibration in hemicelluloses ($H_3C–(C=O)–O–$) and cellulose (Boukir et al. 2019), and 1736 $cm^{-1}$ is correlated to the C=O bonds stretching in acetoxy groups ($H_3C–(C=O)–O–$) of hemicellulose (Porras et al. 2015; Nascimento et al. 2021; Boukir et al. 2019). The two small bands at 2854 $cm^{-1}$ and 2920 $cm^{-1}$ are ascribed to the $CH_2$ symmetrical and asymmetrical stretching in methyl/methylene groups, respectively (Zghari et al. 2017; Nascimento et al. 2021; Boukir et al. 2019). These two bands (2854 $cm^{-1}$ and 2920 $cm^{-1}$) were also reported to represent the wax content (C≡C stretching) in natural fibers (Moshi et al. 2020). The last strong and broad band at 3331 $cm^{-1}$ represents the hydroxyl and carboxylic O–H stretching vibrations in cellulose I (Åkerholm et al. 2004; Jayaramudu et al. 2010; Reddy and Yang 2005; Sugiyama et al. 1991). The observed band centers of natural fiber can vary around ± 16 $cm^{-1}$ from their position for different studies (Zhbankov et al. 2002).

After the delignification treatment, the intensity of bands representing hemicellulose at 1242 $cm^{-1}$, 1371 $cm^{-1}$, and 1736 $cm^{-1}$ were significantly reduced, while bands referring to lignin at the wave numbers of 1513 $cm^{-1}$ and 1602 $cm^{-1}$ completely disappeared. This clearly indicated the reduction of hemicellulose content and the successful removal of lignin.

Additionally, the degree of crystallinity of different samples was compared by the Lateral order index

(LOI) value based on the ratio of the absorbance at 1428 and 893 $cm^{-1}$ (Eq. 6) (Liu et al. 2004).

$$LOI = \frac{a_{1428\,cm^{-1}}}{a_{893\,cm^{-1}}} \quad (6)$$

Here the absorption bands at 1428 and 893 $cm^{-1}$ are assigned to crystalline and amorphous structures of fibers (Korte 2006). The obtained LOI value was 0.32 and 0.52 for JEF and JEF units, respectively. By comparison, these values were lower than that of althaea fiber (0.79), linden (0.96), ferula fibers (0.70) and *Hierochloe Odarata* fiber (1.01) (Dalmis et al. 2020). However, it is important to note that the increased LOI of JEF units indicated a higher degree of crystallinity (Korte 2006), which is also consistent with the relatively high crystallinity of cellulose from stellate JEF units observed under polarized light (Fig. 3c).

## X-ray diffraction analysis

The crystal structures of raw JEF samples and JEF units were evaluated with X-ray diffraction as shown in Fig. 5a. It can be seen that both diffractograms exhibited three obvious peaks around 16°, 22° and 35°, which corresponded to the crystalline planes of (1–10)/(110), (200) and (004), respectively (French 2014; Ling et al. 2019). Specifically, the peak observed around 16° was associated with the cellulose Iβ crystal pattern, which contained overlapping reflections of plane (1–10) and (110) (French 2014; Xia et al. 2020b; Nascimento et al. 2021). After being refined in the software MAUD with the cellulose Iβ crystal pattern (Ling et al. 2019; Saville et al. 2021), these two crystallographic peaks can be distinguished without overlapping in the Rietveld fitted data of JEF units (Fig. 5a). In addition, the absence of "shoulder" peaks nearby the peak (200) can be an indicator for the preferred crystallites orientation of JEF and JEF units cellulosic samples (French 2014, 2020; Ling et al. 2019).

The crystallinity index (CrI) of the JEF and delignified JEF were calculated according to the Segal empirical equation as shown in Eq. (4) (Segal et al. 1959), and the $I_{am}$ and $I_{200}$ was the intensity at 2θ of 18.5° and 22°, respectively. The calculated CrI value of raw JEF and JEF units was 42.5% and 65.1%, respectively. The higher crystallinity observed in JEF units (65.1%) compared to raw JEF indicated the effective partial removal of the amorphous hemicellulose, wax and lignin through the delignification treatment (Chen et al. 2023a). This finding also aligned with the LOI values and FTIR results discussed above (Hashim et al. 2014). Meanwhile the diffractograms peaks between JEF and JEF units shared great similarity, suggesting that the cellulose Iβ crystalline structure of JEF was well-preserved in JEF units during the delignification process (Chen

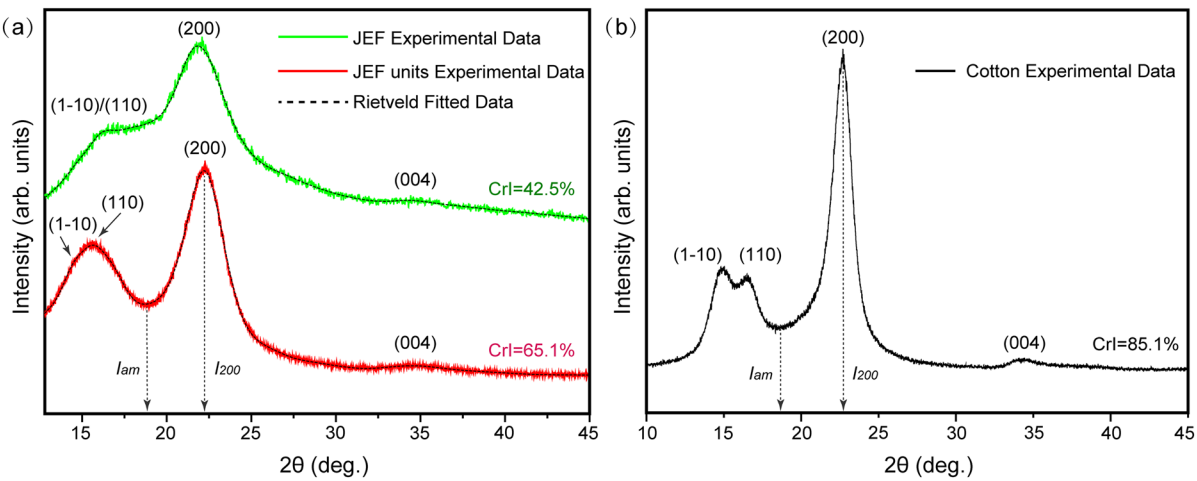


**Fig. 5** **a** X-ray spectra of JEF, JEF units and the corresponding fitting with Rietveld refinement software MAUD; **b** X-ray pattern of cotton

et al. 2023a). As the higher cellulose crystallinity is often recognized as a contributing factor in improving important mechanical characteristics of fibers, including Young's modulus, tensile strength, and hardness (Sanjay et al. 2019), the influence of crystallinity on the stiffness of natural fibers cannot be overstated (Benítez and Walther 2017). As a result, the CrI of cotton was also measured and calculated for comparison here (Fig. 5b) since it is difficult and inaccurate to compare with the reported results obtained under different conditions (Ling et al. 2019; French 2020; Nascimento et al. 2021). Here the CrI of cotton (85.1%) was 2 and 1.3 times that of JEF and JEF units, respectively. The crystallinity of the cellulose fibers obtained from various biomass sources and chemical treatments could vary significantly, ranging from 40 to 91% (Jonoobi et al. 2015). Therefore, the crystallinity of JEF (42.5%) increased substantially from a lower end to a relatively higher end of this range after the deligninfication treatment (65.1%). Besides, the crystallite size (CS) was calculated via Eq. (5) (Scherrer's equation) with the highest intensity peak at 22°. The CS value of raw JEF increased from 2.0 to 2.7 nm (JEF units) after the delignification treatment, rendering its high potential as promising reinforcements in polymeric matrix composites. Moreover, it has been reported that residual amounts of hemicellulose and lignin can potentially enhance the characteristics of resulting composites and even introduce new functionalities (Imani et al. 2019; Song et al. 2018). This suggests that the utilization of delignified JEF units can offer a more cost-competitive option, as they require reduced or less intensive processing, even though it may lower the material's purity. It is important to note that the performance of cellulose materials is not solely dependent on high purity; instead, it varies based on the specific application (Li et al. 2021). This also highlights the significance of considering application-specific requirements when evaluating the suitability of cellulose materials.

## Thermogravimetric analysis

To prevent the degradation of the foams in any potential applications, thermogravimetric analysis was conducted. As shown in Fig. 6a, the thermal degradation process of JEF was presented in four major stages. The first stage occurred in the range of 20–100 °C with a weight loss of 5%, which was regarded as the removal of moisture and wax (Belouadah et al. 2015). Subsequently, when the temperature rose from 160 to 310 °C, the degradation of hemicellulose, partial lignin and the glycosidic links of cellulose occurred as the second and third JEF weight loss (24%) stages with the maximum changing rate at 218.2 °C and 285.2 °C, respectively (Sgriccia and Hawley 2007; Seki et al. 2013; Azwa et al. 2013). Similar thermal degradation stages of hemicellulose (200 ~ 260 °C) and the glycosidic links of cellulose (240 ~ 350 °C) were reported elsewhere (Mohan et al. 2006). Further, the fourth DTG peak at 340.5 °C (weight loss 56%) indicated the direct thermal degradation of cellulose I and α-cellulose (Seki et al. 2013). A similar weight loss was also detected in various natural lignocellulosic fibers such as *Lygeumspartum* (338.7 °C), hemp (308.2 °C), *Cissusquadrangularis* root (328.9 °C) and

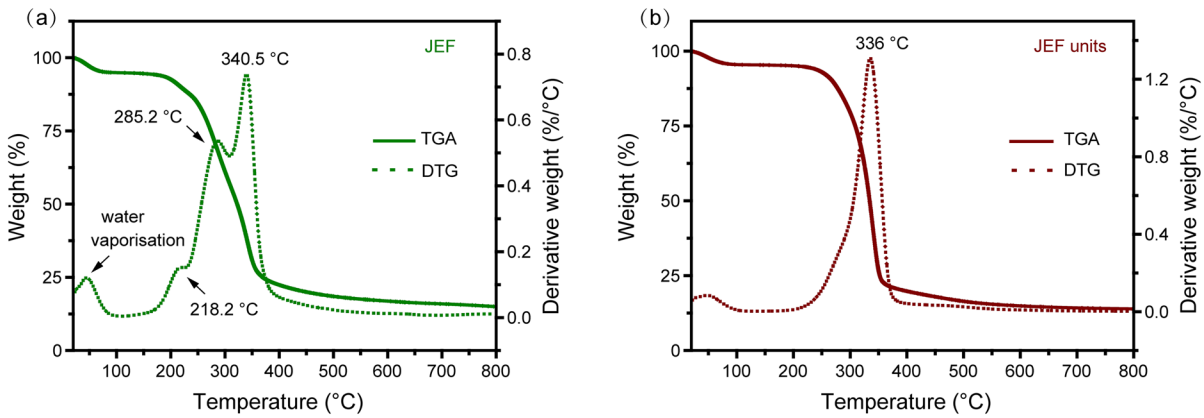


**Fig. 6** TG and DTG curve of **a** raw JEF and **b** JEF units

napier grass (383 °C) (Dhakal et al. 2007; Kommula et al. 2015; Indran and Raj 2015; Belouadah et al. 2015). A residue percentage of 15% was produced at the ending temperature of 800 °C. By comparison, the sample of JEF units had one major weight drop maximizing at 336 °C, which was attributed to the degradation of α-cellulose (Fig. 6b), proving the partial removal of the amorphous hemicellulose and lignin. In addition, previous research has reported that cellulose fibers with lower crystallinity and smaller crystallite size tend to undergo accelerated degradation and exhibit reduced thermal stability (Poletto et al. 2012). Accordingly, the high thermal stability observed in JEF units can be explained by their higher crystallinity and larger crystallite size. In conclusion, thermogravimetric analysis suggests that the raw and delignified JEF were thermally stable below 160 °C and 220 °C, respectively. Therefore, it would be possible to modify the fibers with for instance silane coupling agents for different applications when the reaction was set under the corresponding temperatures (Binoj et al. 2016).

## Tensile and compressive behavior of JEF

Table 3 shows the tensile strength and Young's modulus values of a single JEF with various gauge lengths (10 ~ 50 mm). The average tensile strength of JEF (15.2 ~ 46.6 kPa) were significantly lower than that of extracted fibers from *Juncus effusus* L. stem (113 ± 36 MPa) (Maache et al. 2017), which could be attributed to the vascular vessels and ordered strong sclerenchymatous fibers within the epidermis of the stem (Fig. 2c). Furthermore, the tensile strength of JEF was also lower than most of the natural fibers (≥ 20 MPa) (Indran and Raj 2015), and this low value could be explained by two aspects: chemical composition and microstructures. In terms of chemical composition, the varying contents of cellulose, hemicellulose and lignin in natural fibers have a great impact on their mechanical strength. Cellulose, as the strongest reinforcement material in natural fibers, has the most significant effect on the mechanical properties, followed by lignin (Sreenivasan et al. 2012). In contrast to this, the high hemicellulose content of JEF explains its lower mechanical strength (Sreenivasan et al. 2012). Additionally, from the structural perspective, natural fibers with larger porosity or increased cross-sectional area/diameter typically have lower tensile strength (Fidelis et al. 2013; Wen et al. 2004). This explains the relatively low tensile strength results of JEF as well. Meanwhile, JEF tensile strength values showed an obvious decreasing trend with increased gauge length, and this variability (typical in natural fibers) can be attributed to the different distributions of defects within JEF that are caused by the extraction process (Fidelis et al. 2013).

Compressibility is a vital property for flexible foams. Here, raw JEF exhibited good compressiblity (Fig. 7), which is rare among natural lignocellulosic foams with high porosity (98.08%) (Qiu et al. 2017). As shown in the insets of Fig. 7a, b, JEF is almost fully reversible to its original volume after the first cycle in both two moderate strain uniaxial compressions ($\varepsilon = 30\%$). The volume deformation ratio increased gradually along with the continuing compression cycle, then reached a final value of 12% and 7.5% under the force against the transverse section (direction T) and longitudinal section (direction L), respectively. When the strain was set to a larger value of 60%, JEF still sustained deformations by recovering most of its volume elastically (60% of direction T and 70% of direction L), and revolt the structural fatigue after 10 cycles. This capacity of reversible structural recovery is owed to the highly ordered three-dimensional interconnected configuration of

**Table 3** Mechanical properties of JEF

| Gauge length (mm) | Tensile strength (kPa) | Young's modulus (MPa) | Strain to failure (%) | Cross sectional area ($mm^2$) |
|---|---|---|---|---|
| 10 | 46.6 ± 20.9 | 0.22 ± 0.10 | 35.1 ± 10.5 | 5.8 ± 1.5 |
| 20 | 33.4 ± 10.5 | 0.45 ± 0.48 | 41.2 ± 1.7 | 5.0 ± 2.1 |
| 30 | 24.9 ± 3.9 | 0.52 ± 0.52 | 39.8 ± 10.4 | 5.1 ± 2.6 |
| 40 | 20.4 ± 4.6 | 0.35 ± 0.07 | 53.3 ± 10.2 | 5.7 ± 0.7 |
| 50 | 15.2 ± 7.7 | 0.40 ± 0.23 | 41.7 ± 16.8 | 6.6 ± 0.5 |

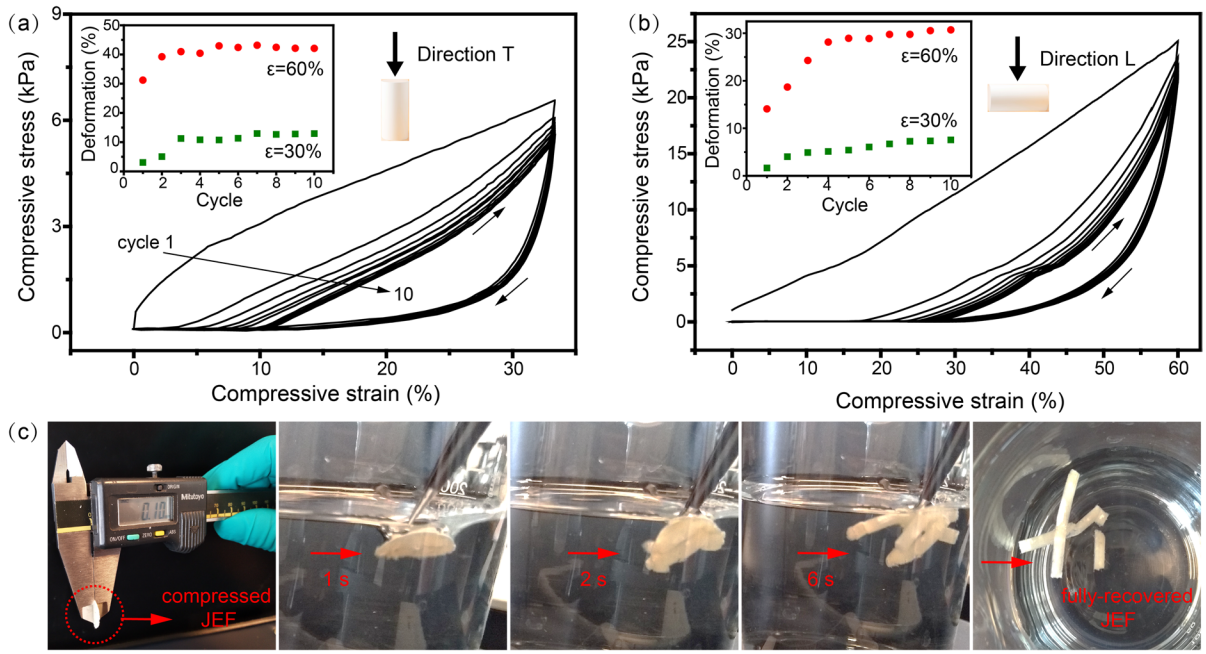


**Fig. 7** Stress-strains curves of JEF **a** at a maximum $\varepsilon$ of 30% along the height of JEF (direction H). Inset, volume deformation ratios initiated via compression for 10 cycles at $\varepsilon$ of 30% and 60%, respectively; **b** at a maximum $\varepsilon$ of 60% along the diameter of JEF (direction D). Inset, volume deformation ratios developed via 10 cycles' compression tests at $\varepsilon$ of 30% and 60%, respectively; **c** the fully-recovered volume of JEF pellet in water

JEF, which could prevent the breaking of linkages between the stellate units, while having the space for densifying at the same time (Gui et al. 2010). Both plateaus at lower $\varepsilon$ and gradually rising slope at high $\varepsilon$ (Fig. 7a, b) can be found in all hysteresis curves, indicating a substantial energy dissipation as a result of the friction between the air or the Teflon mold and the sponge skeletons. In addition, the higher deformation ratios from compression tests along the T direction at the same strain were observed (insets of Fig. 7a, b) indicating less resilient or supporting substances of JEF in these directions, which again corresponds to the stacked layer by layer parallel structure as explained above (Fig. 3f). Interestingly, JEF displayed better structural integrity with the compression force from direction L in accordance with the direction of common environmental stresses (e.g., wind, or animal activities) (Gardiner et al. 2016).

To further investigate the compressibility of the hierarchical structure, JEF was compressed to form a 100 µm thick pellet with 12.75 MPa stress in a dry state (Fig. 7c), in which its original volume shrunk by 99% during the densification. Surprisingly, this densified pellet would instantaneously swell to larger sizes while submerging it in water, and recover most of its thickness within 6 s. This behavior confirmed the interconnected three-dimensionally highly porous structure of JEF. This structure prevents the formation of strong van der Waals interactions even at a densified state, while allowing the absorbed water to refill the open pores very fast and to push back the lignocellulosic cell walls away to their original configurations (Qiu et al. 2017; Wen et al. 2004). Therefore, the structure of JEF holds a great potential as a template in 3D flexible materials' applications.

## Conclusion

In this work, the structural, physico-chemical, mechanical and thermal properties of stellate units of JEF and raw JEF were investigated in-depth. By comparing with other natural cellulosic foams, JEF displayed a distinctive hierarchical interconnected structure consisting of unique hollow stellate units. This unique structure was identified as the key primary

factor contributing to JEF's remarkable characteristics, such as its ultra-lightweight nature (0.017 g/cm$^3$), high porosity (98.08%) and impressive compressibility. The exceptional properties exhibited by JEF offer the possibility for utilizing abundant and problematic aquatic or wetland weeds as alternative sources for versatile 3-dimensional cellulosic foams in a true environmentally sustainable way (from raw materials to manufacturing and final products). By introducing the overlooked aerenchyma plant tissue as a lignocellulosic fiber source and structural template, we have opened up possibilities for various potential applications, including but not limited to oil adsorption, water purification, nanogenerators, and foam structural templates.

**Acknowledgments** The authors are deeply grateful to Dr. Rui Li (group of Polymer Chemistry and Bioengineering, University of Groningen) for his support on the Water Contact Angle measurement and Zhiwen Wang (group of Chemical Technology, University of Groningen) for his support on the chemical composition analysis. The authors are thankful to Jacob Baas (group of Nanostructures of Functional Oxides, University of Groningen) and Léon Rohrbach (group of Green Chemical Reaction Engineering, University of Groningen) for the training and access to the XRD instrument and $N_2$ adsorption-desorption instrument, respectively. The authors are thankful to Joël Benninga (group of Macromolecular Chemistry and New Polymeric Materials, University of Groningen) for writing support.

**Author contributions** QC: conceptualization, methodology, resources, formal analysis, investigation, writing—original draft. JD: methodology, investigation, writing—review & editing. DM: methodology, writing—review & editing. KL: conceptualization, supervision, resources, funding acquisition, writing—review & editing.

**Funding** This work was supported by China Scholarship Council (CSC).

**Availability of data and materials** The data used during this study is available and can be presented upon request.

**Declarations**

**Conflict of interest** The authors declare that they have no competing interests.

**Consent for publication** All authors gave their consent for publication.



## References

Åkerholm M, Hinterstoisser B, Salmén L (2004) Characterization of the crystalline structure of cellulose using static and dynamic FT-IR spectroscopy. Carbohydr Res 339(3):569–578. https://doi.org/10.1016/j.carres.2003.11.012

Anjos O, Pereira H, Rosa ME (2008) Effect of quality, porosity and density on the compression properties of cork. Eur J Wood Wood Prod 66:295–301. https://doi.org/10.1007/s00107-008-0248-2

Azwa ZN, Yousif BF, Manalo AC, Karunasena W (2013) A review on the degradability of polymeric composites based on natural fibres. Mater Des 47:424–442. https://doi.org/10.1016/j.matdes.2012.11.025

Belouadah Z, Ati A, Rokbi M (2015) Characterization of new natural cellulosic fiber from *Lygeum spartum* L. Carbohydr Polym 134:429–437. https://doi.org/10.1016/j.carbpol.2015.08.024

Benítez AJ, Walther A (2017) Cellulose nanofibril nanopapers and bioinspired nanocomposites: a review to understand the mechanical property space. J Mater Chem A 5:16003–16024. https://doi.org/10.1039/c7ta02006f

Binoj JS, Raj RE, Sreenivasan VS, Thusnavis GR (2016) Morphological, physical, mechanical, chemical and thermal characterization of sustainable Indian Areca fruit husk fibers (*Areca catechu* L.) as potential alternate for hazardous synthetic fibers. J Bionic Eng 13:156–165. https://doi.org/10.1016/S1672-6529(14)60170-0

Bismarck A, Aranberri-Askargorta I, Springer J, Lampke T, Wielage B, Stamboulis A, Shenderovich I, Hans-Heinrich L (2002) Surface characterization of flax, hemp and cellulose fibers; surface properties and the water uptake behavior. Polym Compos 23(5):872–894. https://doi.org/10.1002/pc.10485

Blossfeld S, Gansert D, Thiele B, Kuhn AJ, Lösch R (2011) The dynamics of oxygen concentration, pH value, and organic acids in the rhizosphere of *Juncus* spp. Soil Biol Biochem 43:1186–1197. https://doi.org/10.1016/j.soilbio.2011.02.007

Borrega M, Ahvenainen P, Serimaa R, Gibson L (2015) Composition and structure of balsa (*Ochroma pyramidale*) wood. Wood Sci Technol 49:403–420. https://doi.org/10.1007/s00226-015-0700-5

Boukir A, Fellak S, Doumenq P (2019) Structural characterization of *Argania spinosa* Moroccan wooden artifacts during natural degradation progress using infrared spectroscopy (ATR-FTIR) and X-ray diffraction (XRD). Heliyon 5(9):e02477. https://doi.org/10.1016/j.heliyon.2019.e02477

Budtova T (2019) Cellulose II aerogels: a review. Cellulose 26:81–121. https://doi.org/10.1007/s10570-018-2189-1

Chabannes M, Ruel K, Yoshinaga A, Chabbert B, Jauneau A, Joseleau JP, Boudet AM (2001) In situ analysis of lignins in transgenic tobacco reveals a differential impact of individual transformations on the spatial patterns of lignin deposition at the cellular and subcellular levels. Plant J 28:271–282. https://doi.org/10.1046/j.1365-313X.2001.01159.x

Chaiarrekij S, Apirakchaiskul A, Suvarnakich K, Kiatkamjornwong S (2011) Kapok I: characteristics of kapok fiber as a potential pulp source for papermaking. BioResources 7:475–488

Chen Q, Zhao T, Wang M, Wang J (2013) Studies of the fibre structure and dyeing properties of *Calotropis gigantea*, kapok and cotton fibres. Color Technol 129:448–453. https://doi.org/10.1111/cote.12051

Chen X, Yang S, Chen T, Ge Y, Ren M, Shen H, Kuang Y, Lai L, Chang J, Zhang Y (2023a) Highly mesoporous and compressible sugarcane aerogel via top-down nanotechnology as effective and reusable oil absorbents. Cellulose 30:1057–1072. https://doi.org/10.1007/s10570-022-04949-0

Chen Q, Li WJ, Yan F, Maniar D, Dijken J, Petra R, Pei Y, Loos K (2023b) Lightweight triboelectric nanogenerators based on hollow stellate cellulose films derived from Juncus effusus L. aerenchyma. Adv Funct Mater 2304801. https://doi.org/10.1002/adfm.202304801

Colom X, Carrillo F, Nogués F, Garriga P (2003) Structural analysis of photodegraded wood by means of FTIR spectroscopy. Polym Degrad Stab 80(3):543–549. https://doi.org/10.1016/S0141-3910(03)00051-X

Conrad CM (1944) Determination of wax in cotton fiber: a new alcohol extraction method. Ind Eng Chem Anal Ed 16(12):745–748. https://doi.org/10.1021/i560136a007

Cruz G, Monteiro PAS, Braz CEM, Júnior PS, Polikarpov I, Crnkovic PM (2013) Investigation of porosity, wettability and morphology of the chemically pretreated sugarcane bagasse. In: Proceedings of the 22nd International Congress of Mechanical Engineering. Ribeirão Preto, SP, Brazil, pp 10116–10127

Cunha AG, Gandini A (2010) Turning polysaccharides into hydrophobic materials: a critical review. Part 2. Hemicelluloses, chitin/chitosan, starch, pectin and alginates. Cellulose 17:1045–1065. https://doi.org/10.1007/s10570-010-9435-5

Dalmis R, Köktaş S, Seki Y, Kılınç AÇ (2020) Characterization of a new natural cellulose based fiber from *Hierochloe Odarata*. Cellulose 27:127–139. https://doi.org/10.1007/s10570-019-02779-1

Datiles WCP, Herrera MU, Manalo RD, Maguyon-Detras MC, Futalan CCM, Balela MDL (2021) Kapok-cotton carbon sponges for oil recovery. IOP Conf Ser Earth Environ Sci 812:012014. https://doi.org/10.1088/1755-1315/812/1/012014

Dhakal HN, Zhang ZY, Richardson MOW (2007) Effect of water absorption on the mechanical properties of hemp fibre reinforced unsaturated polyester composites. Compos Sci Technol 67:1674–1683. https://doi.org/10.1016/j.compscitech.2006.06.019

Dou J, Paltakari J, Paltakari LS, Paltakari T (2019) Novel insight into the separation and composite utilization of sclerenchyma fiber bundles of willow bark. ACS Sustain Chem Eng 7(3):2964–2970. https://doi.org/10.1021/acssuschemeng.8b04001

Driemeier C, Oliveira MM, Mendes FM, Gómez EO (2011) Characterization of sugarcane bagasse powders. Powder Technol 214:111–116. https://doi.org/10.1016/j.powtec.2011.07.043

Elseify LA, Midani M, El-Badawy AA, Awad S, Jawaid M (2022) Comparative study of long date palm (*Phoenix dactylifera* L.) midrib and spadix fibers with other commercial leaf fibers. Cellulose 30:1927–1942. https://doi.org/10.1007/s10570-022-04972-1

Eltahir AS, AbuEReish BI (2010) Leaf and stem anatomy of *Cymbopogon citratus* and *Cymbopogon schoenanthus* in Sudan. J Chem Pharm Res 2(4):766–771. https://doi.org/10.13140/RG.2.2.14616.60165

Ervin GN, Wetzel RG (2002) Influence of a dominant macrophyte, *Juncus effusus*, on wetland plant species richness, diversity, and community composition. Oecologia 130:626–636. https://doi.org/10.1007/s00442-001-0844-x

Fauziyah M, Widiyastuti W, Balgis R, Setyawan H (2019) Production of cellulose aerogels from coir fibers via an alkali–urea method for sorption applications. Cellulose 26:9583–9598. https://doi.org/10.1007/s10570-019-02753-x

Fidelis MEA, Pereira TVC, Gomes OFM, Silva FA, Filho RDT (2013) The effect of fiber morphology on the tensile strength of natural fibers. J Mater Res Technol 2(2):149–157. https://doi.org/10.1016/j.jmrt.2013.02.003

Fiore V, Scalici T, Valenza A (2014) Characterization of a new natural fiber from *Arundo donax* L. as potential reinforcement of polymer composites. Carbohydr Polym 106:77–83. https://doi.org/10.1016/j.carbpol.2014.02.016

Fredon E, Granet R, Zerrouki R, Krausz P, Saulnier L, Thibault JF, Rosier J, Petit C (2002) Hydrophobic films from maize bran hemicelluloses. Carbohydr Polym 49(1):1–12. https://doi.org/10.1016/S0144-8617(01)00312-5

French AD (2014) Idealized powder diffraction patterns for cellulose polymorphs. Cellulose 21:885–896. https://doi.org/10.1007/s10570-013-0030-4

French AD (2020) Increment in evolution of cellulose crystallinity analysis. Cellulose 27:5445–5448. https://doi.org/10.1007/s10570-020-03172-z

Gabrielii I, Gatenholm P, Glasser WG, Jain RK, Kenne L (2000) Separation, characterization and hydrogel-formation of hemicellulose from aspen wood. Carbohydr Polym 43(4):367–374. https://doi.org/10.1016/S0144-8617(00)00181-8

Gardiner B, Berry P, Moulia B (2016) Review: wind impacts on plant growth, mechanics and damage. Plant Sci 245:94–118. https://doi.org/10.1016/j.plantsci.2016.01.006

Gowthaman S, Nakashima K, Kawasaki S (2018) A state-of-the-art review on soil reinforcement technology using natural plant fiber materials: past findings, present trends and future directions. Materials 11(4):553. https://doi.org/10.3390/ma11040553

Gui X, Wei J, Wang K, Cao A, Zhu H, Jia Y, Shu Q, Wu D (2010) Carbon nanotube sponges. Adv Mater 22(5):617–621. https://doi.org/10.1002/adma.200902986

Guimarães JL, Frollini E, Silva CG, Wypych F, Satyanarayana KG (2009) Characterization of banana, sugarcane bagasse and sponge gourd fibers of Brazil. Ind Crops Prod 30:407–415. https://doi.org/10.1016/j.indcrop.2009.07.013

Guna V, Ilangovan M, Anantha Prasad MG, Reddy N (2017) Water hyacinth: a unique source for sustainable materials and products. ACS Sustain Chem Eng 5:4478–4490. https://doi.org/10.1021/acssuschemeng.7b00051

Guo X, Liu M, Zhong H, Li P, Zhang C, Wei D, Zhao T (2020) Potential of *Myriophyllum aquaticum* for phytoremediation of water contaminated with tetracycline antibiotics and copper. J Environ Manag 270:110867–110999. https://doi.org/10.1016/j.jenvman.2020.110867

Hashim SNAS, Zakaria S, Jaafar SNS, Hua CC (2014) Purification of empty fruit bunch (EFB) and kenaf soda lignin with acidified water. AIP Conf Proc 1614(1):129–135. https://doi.org/10.1063/1.4895184

Hermans PH, Weidinger A (1948) Quantitative X-ray investigations on the crystallinity of cellulose fibers. A background analysis. J Appl Phys 19:491–506. https://doi.org/10.1063/1.1698162

Hinchliff CE, Roalson EH (2009) Stem architecture in *Eleocharis* subgenus *Limnochloa* (Cyperaceae): evidence of dynamic morphological evolution in a group of pantropical sedges. Am J Bot 96:1487–1499. https://doi.org/10.3732/ajb.0800252

Hsieh YL, Thompson J, Miller A (1996) Water wetting and retention of cotton assemblies as affected by alkaline and bleaching treatments. Textile Res J 66(7):456–464. https://doi.org/10.1177/004051759606600707

Huang X, Kocaefe D, Kocaefe Y, Boluk Y, Pichette A (2012) Study of the degradation behavior of heat-treated jack pine (*Pinus banksiana*) under artificial sunlight irradiation. Polym Degrad Stab 97(7):1197–1214. https://doi.org/10.1016/j.polymdegradstab.2012.03.022

Imani M, Ghasemian A, Dehghani-Firouzabadi MR, Afra E, Borghei M, Johansson LS, Gane PAC, Rojas OJ (2019) Coupling nanofibril lateral size and residual lignin to tailor the properties of lignocellulose films. Adv Mater Interf 6:1900770. https://doi.org/10.1002/admi.201900770

Indran S, Raj RE (2015) Characterization of new natural cellulosic fiber from *Cissus quadrangularis* stem. Carbohydr Polym 117:392–399. https://doi.org/10.1016/j.carbpol.2014.09.072

Jain RK, Sjöstedt M, Glasser WG (2001) Thermoplastic xylan derivatives with propylene oxide. Cellulose 7:319–336. https://doi.org/10.1023/A:1009260415771

Jaouadi M, M'sahli S, Sakli F (2009) Optimization and characterization of pulp extracted from the *Agave americana* L. fibers. Text Res J 79:110–120. https://doi.org/10.1177/0040517508090781

Jayaramudu J, Guduri BR, Rajulu AV (2010) Characterization of new natural cellulosic fabric *Grewia tilifolia*. Carbohydr Polym 79:847–851. https://doi.org/10.1016/j.carbpol.2009.10.046

Jebadurai SG, Raj RE, Sreenivasan VS, Binoj JS (2019) Comprehensive characterization of natural cellulosic fiber from *Coccinia grandis* stem. Carbohydr Polym 207:675–683. https://doi.org/10.1016/j.carbpol.2018.12.027

Jonoobi M, Oladi R, Davoudpour Y, Oksman K, Dufresne A, Hamzeh Y, Davoodi R (2015) Different preparation methods and properties of nanostructured cellulose from various natural resources and residues: a review. Cellulose 22:935–969. https://doi.org/10.1007/s10570-015-0551-0

Justin SHFW, Armstrong W (1987) The anatomical characteristics of roots and plant response to soil flooding. New Phytol 106:465–495

Kaczmarek-derda W, Folkestad J, Helgheim M, Netland J, Solhaug KA, Brandsæter LO (2014) Influence of cutting time and stubble height on regrowth capacity of *Juncus effusus* and *Juncus conglomeratus*. Weed Res 54:603–613. https://doi.org/10.1111/wre.12105

Kaczmarek-derda W, Østrem L, Myromslien M, Brandsæter LO, Netland J (2018) Growth pattern of *Juncus effusus* and *Juncus conglomeratus* in response to cutting frequency. Weed Res 59:67–76. https://doi.org/10.1111/wre.12338

Karbowiak T, Ferret E, Debeaufort F, Voilley A, Cayot P (2011) Investigation of water transfer across thin layer biopolymer films by infrared spectroscopy. J Membr Sci 370:82–90. https://doi.org/10.1016/j.memsci.2010.12.037

Keskinkan O, Goksu MZL, Basibuyuk M, Forster CF (2004) Heavy metal adsorption properties of a submerged aquatic plant (*Ceratophyllum demersum*). Bioresour Technol 92:197–200. https://doi.org/10.1016/j.biortech.2003.07.011

Khan MA, Drzal LT (2004) Characterization of 2-hydroxyethyl methacrylate (HEMA)-treated jute surface cured by UV radiation. J Adhesion Sci Technol 18:381–393. https://doi.org/10.1163/156856104773635481

Kommula VP, Obi Reddy K, Shukla M, Marwala T, Reddy EVS, Rajulu AV (2015) Extraction, modification, and characterization of natural ligno-cellulosic fiber strands from napier grass. Int J Polym Anal Char 21:18–28. https://doi.org/10.1080/1023666X.2015.1089650

Korte S (2006) Processing-property relationships of hemp fibre. Dissertation, University of Canterbury

Lazenby A (1955) Germination and establishment of *Juncus effusus* L.: II. The interaction effects of moisture and competition. J Ecol 43(2):595–605. https://doi.org/10.2307/2257013

Lee KP, Kelly DP, Kennedy GL (1983) Pulmonary response to inhaled Kevlar aramid synthetic fibers in rats. Toxicol Appl Pharmacol 71(2):242–253. https://doi.org/10.1016/0041-008X(83)90341-1

Leite C, Pereira H (2017) Cork-containing barks—a review. Front Mater 3:63. https://doi.org/10.3389/fmats.2016.00063

Li T, Chen CJ, Brozena AH, Zhu JY, Xu LX, Driemeier C, Dai J, Rojas OJ, Isogai A, Wågberg L, Hu LB (2021)

Developing fibrillated cellulose as a sustainable technological material. Nature 590:47–56. https://doi.org/10.1038/s41586-020-03167-7

Likon M, Remškar M, Ducman V, Švegl F (2013) Populus seed fibers as a natural source for production of oil super absorbents. J Environ Manag 114:158–167. https://doi.org/10.1016/j.jenvman.2012.03.047

Lim TT, Huang X (2007) Evaluation of hydrophobicity/oleophilicity of kapok and its performance in oily water filtration: comparison of raw and solvent-treated fibers. Ind Crops Prod 26:125–134. https://doi.org/10.1016/j.indcrop.2007.02.007

Ling Z, Wang T, Makarem M, Cintrón MS, Cheng HN, Kang X, Bacher M, Potthast A, Rosenau T, King H, Delhom CD, Nam S, Edwards JV, Kim SH, Xu F, French AD (2019) Effects of ball milling on the structure of cotton cellulose. Cellulose 26:305–328. https://doi.org/10.1007/s10570-018-02230-x

Liu W, Mohanty AK, Drzal LT, Askel P, Misra M (2004) Effects of alkali treatment on the structure, morphology and thermal properties of native grass fibers as reinforcements for polymer matrix composites. J Mater Sci 39:1051–1054

Liu Y, Huang Y, Huang Q, Fan Li, Liu XM (2021) Liquid-phase deposition functionalized wood sponges for oil/water separation. J Mater Sci 56:19075–19092. https://doi.org/10.1007/s10853-021-06440-w

Lo TY, Cui HZ, Leung HC (2004) The effect of fiber density on strength capacity of bamboo. Mater Lett 58(21):2595–2598. https://doi.org/10.1016/j.matlet.2004.03.029

Luz FS, Paciornik S, Monteiro SN, Silva LC, Tommasini FJ, Candido VS (2017) Porosity assessment for different diameters of coir lignocellulosic fibers. JOM 69:2045–2051. https://doi.org/10.1007/s11837-017-2528-y

Maache M, Bezazi A, Amroune S, Scarpa F, Dufresne A (2017) Characterization of a novel natural cellulosic fiber from *Juncus effusus* L. Carbohydr Polym 171:163–172. https://doi.org/10.1016/j.carbpol.2017.04.096

Maepa CE, Jayaramudua J, Okonkwo JO, Ray SS, Sadiku ER, Ramontja J (2015) Extraction and characterization of natural cellulose fibers from maize tassel. Int J Polym Anal Charact 20(2):99–109. https://doi.org/10.1080/1023666X.2014.961118

Mahmood Q, Zheng P, Siddiqi MR, Ejaz I, Rashid AM, Yousaf H (2005) Anatomical studies on water hyacinth (*Eichhornia crassipes* (Mart.) Solms) under the influence of textile wastewater. J Zhejiang Univ Sci B 6:991–998. https://doi.org/10.1631/jzus.2005.B0991

Manian AP, Cordin M, Pham T (2021) Extraction of cellulose fibers from flax and hemp: a review. Cellulose 28:8275–8294. https://doi.org/10.1007/s10570-021-04051-x

Manimaran P, Senthamaraikannan P, Sanjay MR, Marichelvam MK, Jawaid M (2018) Study on characterization of *Furcraea foetida* new natural fiber as composite reinforcement for lightweight applications. Carbohydr Polym 181:650–658. https://doi.org/10.1016/j.carbpol.2017.11.099

Meng J, Guan H, Dai X, Wang X (2021) Amino-functionalized wood aerogel for efficient removal of copper ions from water. Int J Polym Sci 2021:1–8. https://doi.org/10.1155/2021/4913226

Miranda-Valdez IY, Coffeng S, Zhou Y, Viitanen L, Hu X, Jannuzzi L, Puisto A, Kostianien MA, Mäkinen T, Koivisto J, Alava MK (2023) Foam-formed biocomposites based on cellulose products and lignin. Cellulose 30:2253–2266. https://doi.org/10.1007/s10570-022-05041-3

Mohan D, Pittman CU, Steele PH (2006) Pyrolysis of wood/biomass for bio-oil: a critical review. Energy Fuel 20(3):848–889. https://doi.org/10.1021/ef0502397

Mohanty AK, Misra M, Hinrichsen G (2000) Biofibres, biodegradable polymers and biocomposites: an overview. Macromol Mater Eng 276:1–24

Mokhena TC, John MJ (2020) Cellulose nanomaterials: new generation materials for solving global issues. Cellulose 27:1149–1194. https://doi.org/10.1007/s10570-019-02889-w

Moshi AAM, Ravindran D, Bharathi SRS, Indran S, Saravanakumar SS, Liu YC (2020) Characterization of a new cellulosic natural fiber extracted from the root of *Ficus religiosa* tree. Int J Biol Macromol 142:212–221. https://doi.org/10.1016/j.ijbiomac.2019.09.094

Narayanasamy P, Balasundar P, Senthil S, Sanjay MR, Siengchin S, Khan A, Asiri AM (2020) Characterization of a novel natural cellulosic fiber from *Calotropis gigantea* fruit bunch for ecofriendly polymer composites. Int J Biol Macromol 150:793–801. https://doi.org/10.1016/j.ijbiomac.2020.02.134

Nascimento HM, Santos A, Duarte VA, Bittencourt PRS, Radovanovic E, Fávaro SL (2021) Characterization of natural cellulosic fibers from *Yucca aloifolia* L. leaf as potential reinforcement of polymer composites. Cellulose 28:5477–5492. https://doi.org/10.1007/s10570-021-03866-y

Noguchi T, Hosobuchi S, Takamiya T, Iimure K, Saito A, Ohtake Y, Yamashita H, Murakami Y, Okuizumi H (2017) A sequence-tagged site marker for identifying the Japanese mat rush (*Juncus effusus*) cultivar "hinomidori." Jpn Agric Res Q 51(1):45–49. https://doi.org/10.6090/jarq.51.45

Pennells J, Godwin ID, Amiralian N, Martin DJ (2020) Trends in the production of cellulose nanofibers from non-wood sources. Cellulose 27:575–593. https://doi.org/10.1007/s10570-019-02828-9

Pereira H (2015) The rationale behind cork properties: a review of structure and chemistry. BioResources 10:1–23. https://doi.org/10.15376/biores.10.3.Pereira

Pereira PHF, Voorwald HCJ, Cioffi MOH, Mulinari DR, Luz SMD, Silva MLCP (2011) Sugarcane bagasse pulping and bleaching: thermal and chemical characterization. BioResources 6(3):2471–2482

Porras A, Maranon A, Ashcroft IA (2015) Characterization of a novel natural cellulose fabric from *Manicaria saccifera* palm as possible reinforcement of composite materials. Compos B Eng 74:66–73. https://doi.org/10.1016/j.compositesb.2014.12.033

Prakash NH, Sarma A, Sarma B (2018) Antibacterial studies of copper deposited water hyacinth fiber using RF plasma sputtering process. Mater Technol 33:621–633. https://doi.org/10.1080/10667857.2018.1483862

Prasad CV, Rao KC, Reddy GV, Rany TS, Yerriswamy B, Subha MCS (2010) Characteristic studies of lignocellulosic fabric *Grewia tenax*. J Nat Fibers 7:194–215. https://doi.org/10.1080/15440478.2010.504048

Poletto M, Zattera AJ, Forte MMC, Santana RMC (2012) Thermal decomposition of wood: influence of wood components and cellulose crystallite size. Bioresour Technol 109:148–153. https://doi.org/10.1016/j.biortech.2011.11.122

Qiu L, Huang B, He Z, Wang YY, Tian ZM, Liu JZ, Wang K, Song JC, Gengenbach TR, Li D (2017) Extremely low density and super-compressible graphene cellular materials. Adv Mater 29:1701553. https://doi.org/10.1002/adma.201701553

Rahmanian V, Pirzada T, Wang S, Khan SA (2021) Cellulose-based hybrid aerogels: strategies toward design and functionality. Adv Mater 33:2102892. https://doi.org/10.1002/adma.202102892

Rajeshkumar G, Devnani GL, Maran JP, Sanjay MR, Siengchin S, Al-Dhabi NA, Ponmurugan K (2021) Characterization of novel natural cellulosic fibers from purple bauhinia for potential reinforcement in polymer composites. Cellulose 28:5373–5385. https://doi.org/10.1007/s10570-021-03919-2

Rajkumar S, Tjong J, Nayak SK, Sain M (2015) Wetting behavior of soy-based resin and unsaturated polyester on surface-modified sisal fiber mat. J Reinf Plast Compos 34:807–818. https://doi.org/10.1177/0731684415580630

Ram F, Biswas B, Torris A, Kumaraswamy G, Shanmuganathan K (2021) Elastic piezoelectric aerogels from isotropic and directionally ice-templated cellulose nanocrystals: comparison of structure and energy harvesting. Cellulose 28:6323–6337. https://doi.org/10.1007/s10570-021-03896-6

Reddy N, Yang Y (2005) Structure and properties of high quality natural cellulose fibers from cornstalks. Polymer 46(15):5494–5500. https://doi.org/10.1016/j.polymer.2005.04.073

Saeed A, Iqbal M (2013) Loofa (*Luffa cylindrica*) sponge: review of development of the biomatrix as a tool for biotechnological applications. Biotechnol Prog 29:573–600. https://doi.org/10.1002/btpr.1702

Salas-Ruiz A, Barbero-Barrera MM, Ruiz-Téllez T (2019) Microstructural and thermo-physical characterization of a water hyacinth petiole for thermal insulation particle board manufacture. Materials 12(4):560. https://doi.org/10.3390/ma12040560

Sanjay MR, Siengchin S, Parameswaranpillai S, Jawaid M, Pruncu CI, Khan A (2019) A comprehensive review of techniques for natural fibers as reinforcement in composites: preparation, processing and characterization. Carbohydr Polym 207:108–121. https://doi.org/10.1016/j.carbpol.2018.11.083

Sanjay MR, Siengchin S, Parameswaranpillai S, Jawaid M, Ozbakkaloglu T (2022) Lignocellulosic fiber reinforced composites: progress, performance, properties, applications, and future perspectives. Polym Compos 43(2):645–691. https://doi.org/10.1002/pc.26413

Saravanakumar SS, Kumaravel A, Nagarajan T, Sudhakar P, Baskaran R (2013) Characterization of a novel natural cellulosic fiber from *Prosopis juliflora* bark. Carbohydr Polym 92:1928–1933. https://doi.org/10.1016/j.carbpol.2012.11.064

Saville AI, Creuziger A, Mitchell EB, Vogel SC, Benzing JT, Klemm-Toole J, Clarke KD, Clarke AJ (2021) MAUD rietveld refinement software for neutron diffraction texture studies of single- and dual-phase materials. Integr Mater Manuf Innov 10:461–487. https://doi.org/10.1007/s40192-021-00224-5

Seddiqi H, Oliaei E, Honarkar H, Jin J, Geonzon LC, Bacabac RG, Klein-Nulend J (2021) Cellulose and its derivatives: towards biomedical applications. Cellulose 28:1893–1931. https://doi.org/10.1007/s10570-020-03674-w

Segal L, Creely JJ, Martin AE, Conrad CM (1959) An empirical method for estimating the degree of crystallinity of native cellulose using the x-ray diffractometer. Textil Res J 29:786–794. https://doi.org/10.1177/004051755902901003

Seki Y, Sarikanat M, Sever K, Durmuşkahya C (2013) Extraction and properties of *ferula communis* (chakshir) fibers as novel reinforcement for composites materials. Compos B Eng 44(1):517–523. https://doi.org/10.1016/j.compositesb.2012.03.013

Seki Y, Selli F, Erdoğan ÜH, Atagür M, Seydibeyoğlu M (2022) A review on alternative raw materials for sustainable production: novel plant fibers. Cellulose 29:4877–4918. https://doi.org/10.1007/s10570-022-04597-4

Sen S, Singh A, Bera C, Roy S, Kailasam K (2022) Recent developments in biomass derived cellulose aerogel materials for thermal insulation application: a review. Cellulose 29:4805–4833. https://doi.org/10.1007/s10570-022-04586-7

Sgriccia N, Hawley MC (2007) Thermal, morphological, and electrical characterization of microwave processed natural fiber composites. Compos Sci Technol 67:1986–1991. https://doi.org/10.1016/j.compscitech.2006.07.031

Shen J, Xie YM, Huang X, Zhou S, Ruan D (2013) Behaviour of luffa sponge material under dynamic loading. Int J Impact Eng 57:17–26. https://doi.org/10.1016/j.ijimpeng.2013.01.004

Singh V, Kendall RJ, Hake K, Ramkumar S (2013) Crude oil sorption by raw cotton. Ind Eng Chem Res 52:6277–6281. https://doi.org/10.1021/ie4005942

Siva R, Valarmathi TN, Palanikumar K, Samrot AV (2020) Study on a Novel natural cellulosic fiber from *Kigelia africana* fruit: characterization and analysis. Carbohydr Polym 244:116494. https://doi.org/10.1016/j.carbpol.2020.116494

Sluiter A, Hames B, Ruiz R, Scarlata C, Sluiter J, Templeton D, Crocker D (2012) Determination of structural carbohydrates and lignin in biomass. Laboratory Analytical Procedure of the National Renewable Energy Laboratory. https://www.nrel.gov/docs/gen/fy13/42618.pdf. Accessed 3 July 2019

Song J, Chen C, Zhu S, Zhu M, Dai J, Ray U, Li Y, Kuang Y, Li Y, Quispe N, Yao Y, Gong A, Leiste UH, Bruck HA, Zhu JY, Vellore A, Li H, Minus ML, Jia Z, Martini A, Li T, Hu LB (2018) Processing bulk natural wood into a high-performance structural material. Nature 554:224–228. https://doi.org/10.1038/nature25476

Sreenivasan VS, Somasundaram S, Ravindran D et al (2011) Microstructural, physico-chemical and mechanical characterisation of *Sansevieria cylindrica* fibres—an exploratory investigation. Mater Des 32:453–461. https://doi.org/10.1016/j.matdes.2010.06.004

Sreenivasan VS, Ravindran D, Manikandan V, Narayanasamy R (2012) Influence of fibre treatments on mechanical properties of short *Sansevieria cylindrica*/polyester composites. Mater Des 37:111–121. https://doi.org/10.1016/j.matdes.2012.01.004

Stebbins GL, Khush GS (1961) Variation in the organization of the stomatal complex in the leaf epidermis of monocotyledons and its bearing on their phylogeny. Am J Bot 48:51–59. https://doi.org/10.1002/j.1537-2197.1961.tb11604.x

Sugiyama J, Persson J, Chanzy H (1991) Combined infrared and electron diffraction study of the polymorphism of native celluloses. Macromolecules 24(9):2461–2466

Sun J, Li W, E L, Xu Z, Ma C, Wu Z, Liu S (2019) Ultralight carbon aerogel with tubular structures and n-containing sandwich-like wall from kapok fibers for supercapacitor electrode materials. J Power Sources 438:227030. https://doi.org/10.1016/j.jpowsour.2019.227030

Sun J, Guo H, Ribera J, Wu C, Tu K, Binelli M, Panzarasa G, Schwarze FWMR, Wang ZL, Schwarze I (2020) Sustainable and biodegradable wood sponge piezoelectric nanogenerator for sensing and energy harvesting applications. ACS Nano 14:14665–14674. https://doi.org/10.1021/acsnano.0c05493

Thilagavathi G, Karan PC, Das D (2018) Oil sorption and retention capacities of thermally-bonded hybrid nonwovens prepared from cotton, kapok, milkweed and polypropylene fibers. J Environ Manag 219:340–349. https://doi.org/10.1016/j.jenvman.2018.04.107

Tweed RD, Woodhead N (1946) A consideration of *Juncus effusus* L. and *Juncus conglomeratus* L. J Ecol 33:210–213. https://doi.org/10.2307/2256467

Vinod A, Sanjay MR, Suchart SC, Jyotishkumar P (2020) Renewable and sustainable biobased materials: an assessment on biofibers, biofilms, biopolymers and biocomposites. J Clean Prod 258:120978. https://doi.org/10.1016/j.jclepro.2020.120978

Wen CE, Yamada Y, Shimojima K, Chino Y, Hosokawa H, Mabuchi M (2004) Compressibility of porous magnesium foam: dependency on porosity and pore size. Mater Lett 58:357–360. https://doi.org/10.1016/S0167-577X(03)00500-7

Wolverton BC, Mcdonald RC (1979) The water hyacinth: from prolific pest to potential provider. Ambio 8(1):1–9

Xia L, Zhou S, Zhang C, Fu Z, Wang A, Zhang Q, Wang Y, Liu X, Wang X, Xu W (2020a) Environment-friendly *Juncus effusus*-based adsorbent with a three-dimensional network structure for highly efficient removal of dyes from wastewater. J Clean Prod 259:120812. https://doi.org/10.1016/j.jclepro.2020.120812

Xia L, Zhang C, Wang A, Wang Y, Xu W (2020b) Morphologies and properties of *Juncus effusus* fiber after alkali treatment. Cellulose 27:1909–1920. https://doi.org/10.1007/s10570-019-02933-9

Xie Y, Bai H, Liu Z, Chen N (2020) A novel bionic structure inspired by luffa sponge and its cushion properties. Appl Sci 10(7):2584. https://doi.org/10.3390/app10072584

Yang R, Cao Q, Liang Y, Hong S, Xia CL, Wu YJ, Li JZ, Cai LP, Sonne C, Le Q, Lam SS (2020) High capacity oil absorbent wood prepared through eco-friendly deep eutectic solvent delignification. Chem Eng J 401:126150. https://doi.org/10.1016/j.cej.2020.126150

Zaman A, Huang F, Jiang M, Wei W, Zhou ZW (2020) Preparation, properties, and applications of natural cellulosic aerogels: a review. Energy Built Environ 1(1):60–76. https://doi.org/10.1016/j.enbenv.2019.09.002

Zampieri A, Mabande GTP, Selvam T, Schwieger W, Rudolph A, Hermann R, Sieber H, Greil P (2006) Biotemplating of *Luffa cylindrica* sponges to self-supporting hierarchical zeolite macrostructures for bio-inspired structured catalytic reactors. Mater Sci Eng C 26:130–135. https://doi.org/10.1016/j.msec.2005.08.036

Zghari B, Doumenq P, Romane A, Boukir A (2017) GC-MS, FTIR and $^{1}H$, $^{13}C$ NMR structural analysis and identification of phenolic compounds in olive mill wastewater extracted from oued oussefrou effluent (beni mellal-morocco). J Mater Environ Sci 8(12):4496–4509

Zhang X, Wang C, Chai W, Liu X, Xu Y, Zhou S (2017) Kapok fiber as a natural source for fabrication of oil absorbent. J Chem Technol Biotechnol 92:1613–1619. https://doi.org/10.1002/jctb.5155

Zhang C, Xu LH, Ma CY, Wang HM, Zhao YY, Wu YY, Wen JL (2020a) Understanding the structural changes of lignin macromolecules from balsa wood at different growth stages. Front Energy Res 8:181. https://doi.org/10.3389/fenrg.2020.00181

Zhang Q, Ren L, Xiao X, Chen Y, Xia L, Zhao G, Yang H, Wang X, Xu W (2020b) Vertically aligned Juncus effusus fibril composites for omnidirectional solar evaporation. Carbon 156:225–233. https://doi.org/10.1016/j.carbon.2019.09.067

Zhang C, Mo J, Fu Q, Liu Y, Wang S, Nie S (2021) Wood-cellulose-fiber-based functional materials for triboelectric nanogenerators. Nano Energy 81:105637. https://doi.org/10.1016/j.nanoen.2020.105637

Zhbankov RG, Firsov SP, Buslov DK, Nikonenko NA, Marchewka MK, Ratajczak H (2002) Structural physico-chemistry of cellulose macromolecules. Vibrational spectra and structure of cellulose. J Mol Struct 614(1–3):117–125. https://doi.org/10.1016/S0022-2860(02)00252-1

Zheng Y, Zhu Y, Wang A, Hu H (2016) Potential of *Calotropis gigantea* fiber as an absorbent for removal of oil from water. Ind Crops Prod 83:387–390. https://doi.org/10.1016/j.indcrop.2016.01.009